

Interprotein Electron Transfer Biohybrid System for Photocatalytic H₂

Production

Udita Brahmachari, P. Raj Pokkuluri, David M. Tiede, Jens Niklas, Oleg G. Poluektov, Karen L.

Mulfort, Lisa M. Utschig*

Chemical Sciences and Engineering Division, Argonne National Laboratory, Lemont, IL 60439,

USA

Corresponding author: Dr. Lisa M. Utschig, Chemical Sciences and Engineering Division,

Argonne National Laboratory, Lemont, IL 60439, USA.

Email: utschig@anl.gov

Tel: +1-630-252-3544

Abstract

Worldwide there is a large research investment in developing solar fuel systems as clean and sustainable sources of energy. The fundamental mechanisms of natural photosynthesis can provide a source of inspiration for these studies. Photosynthetic reaction center (RC) proteins capture and convert light energy into chemical energy that is ultimately used to drive oxygenic water-splitting and carbon fixation. For the light energy to be used, the RC communicates with other donor/acceptor components via a sophisticated electron transfer scheme that includes electron transfer reactions between soluble and membrane bound proteins. Herein, we reengineer an inherent interprotein electron transfer pathway in a natural photosynthetic system to make it photocatalytic for aqueous H₂ production. The native electron shuttle protein ferredoxin (Fd) is used as a scaffold for binding of a ruthenium photosensitizer and H₂ catalytic function is imparted to its partner protein, ferredoxin NADP⁺-reductase (FNR), by attachment of cobaloxime molecules. We find that this 2-protein biohybrid system produces H₂ in aqueous solutions via light-induced interprotein electron transfer reactions (TON >2500 H₂/FNR), providing insight about using native protein-protein interactions as a method for fuel generation.

Keywords: Interprotein electron transfer, biohybrid, solar hydrogen, ferredoxin, ferredoxin-NADP⁺-reductase, solar fuel, photosynthetic electron transfer

Introduction

Sunlight is a clean and abundant source of energy. An efficient way to store solar energy is in energy-rich chemical bonds of molecules, such as H₂ (Lewis and Nocera 2006; Lewis 2007). When created using the energy from sunlight, H₂ is considered a solar fuel. Nature provides a model for this in the photosynthetic reaction center (RC) proteins that capture and convert the sun's energy and power the rearrangement of the bonds of water to form oxygen and the biological equivalent of hydrogen, NADPH, which is used in carbon fixation. Therefore, using what we know of the high quantum efficiency and self-repair capabilities of natural photosynthesis, there is growing interest in the development of biohybrid architectures for the photocatalytic production of H₂ using visible light and water (Utschig et al. 2015; Mulfort and Utschig 2016). There are several strategies for solar H₂ generation that couple light-driven RC chemistry to the direct synthesis of H₂ in hybrid systems where abiotic H₂ production capabilities have been inserted into the RC protein framework (Utschig et al. 2015). In particular, hybrids of the Photosystem I (PSI) RC linked to hydrogenase (Ihara et al. 2006; Lubner et al. 2010; Lubner et al. 2011), Pt nanoclusters (Greenbaum 1988; Iwuchukwu et al. 2010), Pt nanoparticles (Grimme et al. 2008; Utschig et al. 2011a), and molecular first row transition metal catalysts (Utschig et al. 2011a; Silver et al. 2013) have been successful for light-driven H₂ generation from water. This work has led to the integration of abiotic H₂ catalysts within intact thylakoid membranes to achieve complete solar water splitting via the native photosynthetic Z-scheme electron transport chain (Utschig et al. 2018).

In addition to PSI hybrids, small proteins can be used as a foundation to generate biohybrid architectures that replicate the essential design features of RCs by combining protein scaffolds with tailored abiotic cofactors and synthetically-tuned photosensitizers to produce H₂ from light in

aqueous solutions (Soltau et al. 2015; Soltau et al. 2016; Soltau et al. 2017). Biohybrids built from proteins smaller and less complex than RCs provide a more straightforward system in which to monitor photoinduced electron transfer kinetics and charge recombination pathways as related to H₂ catalysis. Without the optimized RC light capture and conversion capabilities, the small hybrids exhibit low quantum efficiencies for the two-electron process of H₂ production, yet synthetic molecular chemistry imparts important creativity and tunability in the hybrid design strategy that has yielded important information about sequential charge separation, electron transfer pathways and intermediate states in photocatalysis (Soltau et al. 2015; Soltau et al. 2016; Soltau et al. 2017).

In this report, we investigate light-driven *inter*protein electron transfer in small biohybrid designs as an approach for the direct synthesis of energy rich compounds. Biological electron transfer between proteins is involved in a variety of physiologically important processes. In photosynthesis, interprotein electron transfer reactions between mobile charge carrier proteins and integral membrane proteins is essential for utilizing the photon energy captured by RCs. For example, PSI catalyzes light-driven electron transfer across the thylakoid membrane from plastocyanin located in the lumen to ferredoxin in the stroma. Ferredoxin then shuttles electrons to ferredoxin-NADP⁺ reductase (FNR). We look at adding synthetic complexes to the Fd-FNR subset of the native photosynthetic electron transport chain to explore the feasibility and utility of incorporating interprotein electron transfer in photocatalytic hydrogen production schemes.

Materials and methods

FNR overexpression and purification

A synthetic gene encoding FNR domain from *Anabaena* PCC 7119 (Uniprot P21890; amino acids 137-440) was designed using optimized codons for high expression in an *E. coli* host strain by a proprietary algorithm at GenScript (Piscataway, NJ). The synthetic DNA was purchased from GenScript and was cloned into the protein expression vector pMCSG68 developed at the Midwest Center for Structural Genomics (MCSG) at the Argonne National Laboratory, IL. A N-terminal His₆-tag was introduced to enable isolation by immobilized metal affinity chromatography (IMAC). The His₆-tag can be cleaved efficiently by TEV protease.

A surface exposed cysteine residue was introduced by replacing glycine at position 402 in FNR (G265C in the numbering adopted in the PDB deposited structure, 1GJR) using site-directed mutagenesis. The substitution was verified by DNA sequencing. The FNR G402C mutant was expressed in *E. coli* (BL21 Gold) and purified using Ni-affinity column chromatography. Following the first IMAC purification step, the His₆-tag was cleaved using TEV protease, and the reaction mixture was further purified using a second IMAC column to separate the cysteine mutant from any tag-uncleaved mutant protein and the protease (both containing His₆-tag). Following purification, the buffer was exchanged to 20 mM HEPES pH 8.0, 250 mM NaCl, 2mM DTT by repeated dilution and concentration using Amicon ultra-15 centrifugal filter. The purity of the G402C FNR mutant was assessed by a single band on an SDS-PAGE gel. The purified FNR G402C mutant was used for all experiments in this study. It will be referred to as FNR henceforth for simplicity.

UV-Vis spectroscopy of the purified FNR protein showed low incorporation of the native FAD cofactor (Figure S1). The apo-FNR was reconstituted with FAD (Sigma-Aldrich) by incubation of a 0.5-1 mM solution of FNR in 20 mM HEPES pH 8.0 and 250 mM NaCl with 4-6 mol equiv. FAD overnight at 4 °C. Unbound FAD was removed by extensive washing with 10000 MWCO

filtration devices until the filtrate was colourless. FAD reconstitution was verified by UV-Vis spectroscopy (Figure S1). FNR concentration was determined by extinction coefficient at 456 nm of $10,740 \text{ M}^{-1} \text{ cm}^{-1}$ and verified separately by Bradford assays using the Bio-Rad Protein Assay Dye Reagent.

Preparation of Fd-RuPS and FNR-Co hybrids

Chemicals for the synthesis of $\text{Co}(\text{dmgBF}_2)_2 \cdot 2\text{H}_2\text{O}$ (CoBF_2) and $[\text{Ru}(4\text{-CH}_2\text{Br-4}'\text{-CH}_3\text{-2,2}'\text{-bpy})(\text{bpy})_2] \cdot 2\text{PF}_6$ (RuPS) were purchased from Sigma-Aldrich and used as received. The CoBF_2 catalyst and RuPS were synthesized and characterized according to published methods (Bakac and Espenson 1984; Gould et al. 1991; Sun et al. 1997). The Fd-RuPS hybrid was prepared using *Spinacia oleracea* ferredoxin from Sigma-Aldrich. $80 \mu\text{M}$ Fd in 20 mM HEPES pH 8.0 was incubated with 4 mol equiv. of RuPS (7 mM stock in DMSO) overnight at $4 \text{ }^\circ\text{C}$. To remove unbound RuPS, the samples were concentrated with Amicon 3000 MWCO filtration devices and repeatedly diluted and washed 4 times with 20 mM HEPES pH 8.0. Fd concentration was determined using the extinction coefficient at 422 nm of $9,600 \text{ M}^{-1} \text{ cm}^{-1}$. ApoFd was prepared by treatment of spinach Fd with 3% trichloroacetic acid and dithiothreitol as previously reported (Utschig et al. 2018). ApoFd (Figure S2) protein concentration was determined by the Bradford method. The Ru-ApoFd hybrid was made by the same procedure as the Fd-RuPS hybrid. Bradford assays were used to determine the concentrations of Fd-RuPS and ApoFd-RuPS.

Both ApoFNR- CoBF_2 and FAD reconstituted FNR- CoBF_2 hybrids were prepared by addition of 10 mol equiv. of CoBF_2 (freshly prepared $1.5\text{-}3 \text{ mM}$ stock in DMSO) to a $20\text{-}50 \mu\text{M}$ solution of FNR in 20 mM HEPES pH 8.0. The mixture was incubated overnight at 4°C followed by repeated concentration/wash steps with 20 mM HEPES pH 8.0 through Amicon 10000 MWCO filtration devices to remove unbound catalyst.

Photosensitizer and catalyst protein binding ratios were determined using inductively coupled plasma atomic emission spectroscopy (ICP-AES) with a Thermo Scientific iCAP6000 spectrometer. Dilute protein hybrid solutions were analyzed for the appropriate metal ion, Co, Fe, and/or Ru. The metal concentrations determined by ICP-AES were then compared to the protein concentrations of each specific sample as determined by UV-Vis analysis.

NADP⁺ Reduction

Light-dependent NADPH reduction by ApoFNR, FNR, and FNR-CoBF₂ hybrids was measured using PSI isolated from *S. leopoliensis* and then purified. (Mosebach et al. 2017) PSI concentration was determined by chlorophyll content in 100% methanol by measuring the optical density at 664 nm. Samples with 60 nM PSI monomer contained 20 mM Tricine-KOH (pH 7.3), 3 mM MgCl₂, 2 mM sodium ascorbate, 60 μM DCPIP, 10 μM cyt c₆ (*S. lividus*), 4 μM Fd, 0.5 mM NADP⁺ (Sigma-Aldrich), and 0.5 μM FNR. Absorption at 340 nm (and at 390 nm) was measured prior to and during specific time points of illumination with a 300 W Xe lamp (Perkin-Elmer). The light was extensively filtered using a 500 nm long-pass filter, a short-pass filter (KG-2, Schott) and a 29 cm water filter.

EPR Experiments

ApoFNR-CoBF₂ and FNR-CoBF₂ samples were prepared as described above, and concentrated to 100-200 μM protein in 20 mM HEPES pH 8.0 buffer with 100 mM sodium ascorbate. Samples were prepared in quartz EPR tubes in a nitrogen box. A Bruker ELEXSYS II E500 EPR spectrometer (Bruker Biospin, Rheinstetten, Germany) equipped with a TE₁₀₂ rectangular resonator (Bruker ER4102ST) and a helium gas-flow cryostat (ICE Oxford, U.K.) was used for CW X-band EPR measurements. An ITC (Oxford Instruments, U.K.) was used for temperature

control. After data collection of the FNR-CoBF₂ sample, 170 μ M Fd was added to the sample, and a CW spectrum obtained. Data processing was performed using Xepr (Bruker Biospin, Rheinstetten, Germany) and MatlabTM 7.11.2 (MathWorks) environment. The magnetic parameters were obtained by simulation with EasySpin (Stoll and Schweiger 2006).

Photocatalytic H₂ Production

Photocatalytic H₂ generation experiments were performed with a blue LED (455 nm) focused on a N₂-purged, sealed 5.3 ml spectrophotometer cell with a path length of 1.0 cm. FNR-cobaloxime samples were diluted to a final concentration of 0.1-2 μ M protein in 3 ml 10 mM MES buffer (pH 6.1) and 100 mM sodium ascorbate as a sacrificial electron donor. 8 μ M Fd-RuPS hybrid was added to this mixture. The output from the LED was focused using a Thorlabs Aspheric condenser lens to a radius of 3.5 cm on the sample cell. The LED was positioned 10 cm from the sample. The Thorlabs powersource (DC2200) was set to 950 mA. Samples (200 μ l) were taken from the headspace every 30 - 60 min and analyzed for H₂ with a Varian CP-4900A micro gas chromatograph with a 10 m 5 Å molecular sieves column with a thermal conductivity detector and UHP N₂ carrier gas. Calibration curves for H₂ concentrations were determined using injections of a known standard of 3 % H₂ in N₂.

Results and Discussion

As demonstrated in our previous work, (Soltau et al. 2015) the ruthenium photosensitizer, RuPS (Figure 1A) forms a covalent bond via a thiolate linkage to Cys18 of *Spinacia oleracea* ferredoxin (Fd). After removal of unbound RuPS by microfiltration, ICP-AES revealed 1.2 ± 0.1 Ru/Fd. The cobaloxime catalyst, CoBF₂ (Figure 1B) coordinates directly with *Anabaena* FNR via Co(II) His

and/or Glu/Asp coordination after overnight incubation. Removal of unbound CoBF₂ and subsequent ICP-AES indicates 1.4 ± 0.3 Co/FNR. To enable intermolecular electron transfer, the Fd-RuPS and FNR-CoBF₂ hybrids were mixed together in a cuvette with the sacrificial electron donor sodium ascorbate under blue LED illumination. Figure 1C shows the proposed schematic for the intermolecular electron transfer reaction to generate hydrogen. A model of the active complex is proposed by aligning the spinach Fd structure (1A70, (Binda et al. 1998)) with the *Anabaena* FNR:Ferredoxin complex structure (1EWY, (Morales et al. 2000b)).

The two-hybrid mixture where the photosensitizer molecule is linked to Fd and the catalyst is bound to FNR readily generates H₂ from aqueous solutions under blue LED illumination (Figure 2). The assay conditions of 10 mM MES pH 6.1, 100 mM sodium ascorbate, and 0.1-2 μM protein were those previously found to work best for similar systems (Soltau et al. 2015; Soltau et al. 2017). The ratio of Fd-RuPS to FNR-CoBF₂ was varied to maximize H₂ production. We observed that increasing the ratio Fd-RuPS photosensitizer hybrid to the FNR-CoBF₂ catalyst hybrid dramatically increased the H₂ production. With 4:1 (Figure 2, red triangles), 21:1 (Figure 2, green circles), and 72:1 (Figure 2, black squares) Fd-RuPS:FNR-CoBF₂ ratios, the observed total TONs were 490, 1640, and 2780 TON H₂/FNR, respectively (Table 1). The maximum rates for H₂ production (TOF) were measured to be 110, 330, and 550 mol H₂ (mol FNR)⁻¹ h⁻¹, respectively (Table 1).

The duration of H₂ evolution for this interprotein biohybrid system was tested for the 4:1 Fd-RuPS:FNR-CoBF₂ mixture (Figure S3) over several hours. We observed that H₂ production begins to taper off after 5 hours of illumination (Figure S3, red open triangles). Addition of fresh ascorbate after 25.5 hours of illumination failed to revive H₂ production (Figure S3, black circle), suggesting that accumulation of oxidized ascorbate does not limit the long-term efficiency of this system. In

the literature, recovery of H₂ production has been observed with addition of fresh photosensitizer (Ru(bpy)₃Cl₂) after several hours of illumination (Kohler et al. 2019). Figure S4 shows the absorption spectrum of Ru(bpy)₃Cl₂ under blue LED illumination. The 450 nm MLCT band diminishes in size significantly after extended illumination. A new band at 520 nm appears and eventually dominates the spectrum after 21.5 hours. This indicates a change in the ligand environment of the Ru(II) ion. Based on the literature and the observed changes in the absorption spectrum, we conclude that light-induced decomposition of the RuPS is a limiting factor for long-term H₂ production in our system.

Together, these results show that intermolecular electron transfer is an effective mechanism for photocatalytic H₂ production from biohybrid systems. A significant improvement in TON is achieved compared to corresponding Ru-Fd-CoBF₂ and Ru-apo-flavodoxin-CoBF₂ hybrids that use intramolecular electron transfer (Soltau et al. 2016). The TON also approaches that for the only other reported interprotein biohybrid system, that of PSI and a nickel diphosphine substituted apo-flavodoxin, (Silver et al. 2013) although the TOF of the PSI hybrids remain the fastest to date for molecular catalyst-protein hybrids, (Utschig et al. 2011b) due to the optimized photochemistry of photosynthetic RC proteins. The protein architectures are instrumental in facilitating H₂ production. When the CoBF₂ catalyst (3 μM, no FNR) was mixed with Ru[(bpy)₃]Cl₂ (8 μM, no Fd) and 100 mM ascorbate to match the concentrations used in the protein hybrid photocatalysis, extremely low activity of 10 TON H₂/CoBF₂ was observed following illumination (Table S1) which can be attributed to diffusion limitations. Upon mixing FNR-CoBF₂ with free Ru[(bpy)₃]Cl₂ photosensitizer, 16 TON H₂/FNR was observed with illumination, even though the photosensitizer was added in 4 fold excess of the FNR-CoBF₂. Therefore, very little to no H₂ was observed without either Fd or FNR. Hence, both the Fd and FNR protein structures play a necessary role in enabling

efficient intermolecular electron transfer between the PS and catalyst in this biohybrid system for light-induced H₂ production.

This biohybrid system provides the opportunity to investigate the involvement of intermediate cofactors as electron relays in photocatalysis. The intermolecular electron transfer between the RuPS bound to Fd and the cobaloxime catalyst bound to FNR could take place via the [2Fe-2S] cluster of Fd and/or the FAD cofactor of FNR. Sequential intramolecular electron transfer via the [2Fe-2S] cluster of Fd has been previously observed for a Ru-Fd-Co hybrid (Soltau et al. 2015). To test the mechanism, the [2Fe-2S] cluster of Fd and FAD cofactor of FNR were each removed to form the apo-proteins prior to preparing the corresponding hybrids as detailed in the methods section. The concentrations of the FNR-CoBF₂ and Fd-RuPS hybrids were kept constant at 2 μM and 8 μM, respectively. Therefore, a 4:1 ratio of Fd-RuPS:FNR-CoBF₂ was maintained for these experiments.

Figure 3 presents the H₂ generated by the different combinations of the apo- and native protein hybrids over time. The black squares (Figure 3) represent a mixture of intact Fd-RuPS and FNR-CoBF₂ where 490 TON H₂/FNR was observed. Trichloroacetic acid precipitation to remove the [2Fe-2S] cluster from Fd yielded 0.09 ± 0.02 Fe/ApoFd, similar to an earlier report (Soltau et al. 2015). The Ru content of the ApoFd-RuPS hybrid is similar to the intact Fd-RuPS hybrid (1.1 ± 0.1 Ru/ApoFd). Upon mixing ApoFd-RuPS with FNR-CoBF₂ followed by illumination the maximum activity observed was 490 TON H₂/FNR (Table 1), comparable to that with the native hybrid (Figure 3, green circles), suggesting that the [2Fe-2S] cluster of Fd is not essential for photocatalysis. The purified G402C mutant FNR exhibited very low levels of FAD incorporation and was used as ApoFNR (Figure S1). Upon reaction with the cobaloxime catalyst, it bound 1.8 ± 0.3 Co/ApoFNR which is slightly higher than that observed for FAD reconstituted FNR. When

ApoFNR-CoBF₂ was mixed with Fd-RuPS and assayed for photocatalytic H₂ production, 510 TON H₂/ApoFNR was observed (Figure 3, red open triangles, Table 1). Since the ApoFNR-CoBF₂ and FNR-CoBF₂ exhibit similar H₂ evolution, we infer that FAD cofactor has no effect on the H₂ production. As an additional test, ApoFNR-CoBF₂ and ApoFd-RuFd were mixed together and illuminated. Under these conditions, we observed 740 TON H₂/ApoFNR (Figure 3, blue inverted triangles, Table 1) which is higher than the other three conditions tested. It is possible that the Fd [2Fe-2S] cluster (-0.42 V vs. NHE) (Cammack et al. 1977) and the FNR FAD cofactor (-0.33 V vs. NHE for the semiquinone/hydroquinone couple and -0.35 V vs NHE for the oxidized enzyme/semiquinone couple at pH 7) (Corrado et al. 1996; Faro et al. 2002) are reduced following light excitation of [Ru(bpy)₃]²⁺ to [Ru(bpy)₃]^{2+*} (Ru(II*/III) -0.8 V vs. NHE) (Alstrum-Acevedo et al. 2005)). However, if electron transfer to these sites does occur, it does not appear to impact photoinduced electron transfer between the photosensitizer and catalyst sites. The increase in TON for the dual apo-protein experiments (740 vs 490) would be consistent with non-productive electron transfers to the [2Fe-2S] and/or FAD sites. Overall, however, we conclude that neither the [2Fe-2S] cluster nor the FAD are essential as electron transfer relays between the RuPS and cobaloxime catalyst. These results indicate that both the photoinduced electron transfers proceed directly from Ru of Fd-RuPS to the Co-catalyst on FNR-CoBF₂ (Figure 1C).

In a previous study, intermolecular electron transfer between *Synechocystis* sp. PC 6803 Fd and FNR was achieved using Ru based photosensitizers, one of which was the same as that used in this study (Figure 1A) (Quaranta et al. 2016). The RuPS(s) were covalently bound to Fd via cysteine residues, site specifically mutated into the structure. The electron transfer proceeded via reductive quenching of Ru* to reduce the [2Fe-2S] cluster followed by reduction of the FAD cofactor. For one of the mutants, the measured interprotein intracomplex electron transfer rate was

6500 s⁻¹. This study, as well as our previous small protein hybrid work, (Soltau et al. 2016; Soltau et al. 2017) suggests that most likely a similar reductive quenching mechanism occurs for Ru(II)* in the presence of 100 mM ascorbate in our interprotein electron transfer system. In the native proteins from *Anabaena*, electron transfer rates (k_{et}), of 4600 ± 400 s⁻¹ have been reported (Hurley et al. 2002). Therefore, the rates were comparable between the native Fd to FNR and biohybrid Fd-RuPS to FNR. Planned kinetic studies of the Fd-RuPS/FNR-CoBF₂ system using time-resolved optical spectroscopy will be important for understanding the underlying mechanisms of the interprotein electron transfer processes that facilitate photocatalysis.

Effective electron transfer from Fd to FNR involves formation of an active collision complex. FNR contains a mainly positive patch and electrostatic forces with the negatively charged surface of reduced Fd, an acidic protein, contribute to complex formation preceding electron transfer. (Medina 2009) To test the effect of the protein-protein complex formation on H₂ production via intermolecular electron transfer, the ionic strength of the solution was varied. With no salt addition, 220 TON H₂/FNR was observed (Figure 4, green circles, Table 1). In the presence of 200 mM NaCl, the maximum TON increased to 490 TON H₂/FNR (Figure 4, black squares, Table 1). But with 1 M NaCl, 140 TON H₂/FNR was observed (Figure 4, red triangles, Table 1). So a biphasic salt dependence is observed for the electron transfer reaction. This result matches the literature where analogous salt dependence has been observed for the complex formation between Fd and FNR for effective electron transfer (Martínez-Júlvez et al. 1998).

The electrostatic nature of the interaction between Fd and FNR can explain the observed ionic strength dependence of H₂ production. At low ionic strengths, due to the high surface charge density, the two partners can come together in orientations that are not conducive to electron transfer and fail to reorient themselves. On the other hand, if the ionic strength is too high, the

surface charges are screened too well and complex formation fails to occur. In the literature, a bell-shaped curve is observed for rate of FNR reduction versus ionic strength (Martínez-Júlvez et al. 1998). In our experiments, no salt addition leads to low H₂ production. Addition of some salt (200 mM NaCl) increases the H₂ production but further increase in ionic strength (1 M NaCl) hinders H₂ production.

The mechanism of complex formation followed by electron transfer between Fd and FNR has been studied using several experimental techniques, including site-directed mutagenesis, kinetic measurements among others (Mulo and Medina 2017). A two-step mechanism has been used to explain the observed results. The initial complex formation between reduced ferredoxin and oxidized FNR was characterized by the reversible binding constant, K_d followed by electron transfer in the forward direction characterized by the rate constant, k_{et} . The dissociation constant, K_d for the Fd:FNR complex range from 4-10 μ M. Ionic strength of the solution modulates the affinity between Fd and FNR. The initial encounter is driven by the dipole moment generated due to the charged residues on the surface of Fd and FNR. However, a reorientation is required to position the FAD and [2Fe-2S] clusters for optimal electron transfer. Salt bridges play a role in reorienting the two proteins, where generally negatively charged Fd residues interact with positively charged residues on FNR. Simulations have shown that the rate of complex formation between Fd and FNR is constant over the pH range 6 to 7.5 (Diakonova et al. 2016). Crystal structures of the Fd:FNR complex have also been reported for *Zea mays* (Kurisu et al. 2001) and *Anabaena* (Morales et al. 2000b), where the flavin isoalloxazine and [2Fe-2S] were separated by $<8 \text{ \AA}$. Models proposed on the basis of NMR chemical shifts (Palma et al. 2005) varied from the crystal structure thereby further supporting the idea that within the Fd:FNR complex, multiple Fd orientations are capable of supporting fast interprotein electron transfer.

Based on the crystal structure of *Anabaena* FNR complexed with Fd, the complexation of the two proteins is mediated by a hydrophobic core, net 11 *interprotein* hydrogen bonds and one salt bridge (Morales et al. 2000a; Morales et al. 2000b). The hydrophobic core is comprised of Phe65 on Fd and FNR residues Leu76, Leu78 and Val136. The Fd/FNR residues involved in either direct or water mediated hydrogen bonds are Tyr25/Arg264, Arg42/Arg264, Ser61/Lys293, Ser61/Val300, Asp62/Glu267, Asp62/Thr302, Ser64/Glu301, Ser64/Val136, Asp67/Asn13, Glu94/Lys75. Salt bridge formation occurs between Arg264 of FNR and Asp62 of Fd. The residues that exerted the most dramatic effect on the rate of electron transfer are Phe65, Glu94, and Ser47 on Fd and Leu76, Lys75, and Glu301 on FNR (Hurley et al. 2002). Smaller effects were observed for Asp67 in Fd and Glu139, Leu78, Lys72, and R16 in FNR. Figure S5 shows the sequence alignment between Fd from *Anabaena* and spinach (E92K mutant). Although most of the key residues are conserved, Ser61 (*Anabaena*) is replaced by Asp59 (spinach). Therefore, in our current system (*Anabaena* FNR and spinach Fd) a majority of these interprotein interactions are present which leads to the formation of productive complexes for electron transfer. However, since the [2Fe-2S] cluster on Fd and FAD on FNR are not involved in mediating electron transfer in our biohybrid system, direct structural information on Fd-RuPS and FNR-CoBF₂ is required to clarify the molecular details of the photocatalytic complex.

The FNR binding site of the Co catalyst was characterized using electron paramagnetic resonance (EPR) experiments. The CoBF₂ catalyst has a 3d⁷ EPR active configuration with Co(II) oxidation state (Bakac et al. 1986). EPR spectroscopy can distinguish between nitrogen and oxygen axial coordination of Co(II) (Niklas et al. 2012). Figure 5A (black) presents the EPR spectrum of ApoFNR-CoBF₂ and Figure 5B (red) shows the FNR-CoBF₂ spectrum. Upon comparing the ApoFNR-CoBF₂ and FNR-CoBF₂ spectra, there are differences in the coordination environment

of the CoBF₂ catalyst when bound to the intact FNR versus the ApoFNR. Deconvolution of the spectra followed by simulation (Figure S6) revealed 50% N-coordination and 50% O-coordination for FNR-CoBF₂. This is in contrast to the ApoFNR-CoBF₂ spectrum which corresponds to 85-90% O-coordination and 10-15% N-coordination. There are 8 histidine residues in our FNR structure. One of them is buried and the remaining 7 are solvent exposed and one of them could provide axial coordination to the Co(II) center in FNR-CoBF₂. The stoichiometric nature of catalyst binding to FNR (1.4 ± 0.3 Co/FNR) suggests that 1 histidine provides preferential ligation. In addition to histidine, there are multiple glutamate and aspartate surface residues that can readily bind axially to the cobaloxime. To test whether the CoBF₂ binds near the Fd docking site, Fd was added to the FNR-CoBF₂ sample. The EPR spectrum remains unaffected upon Fd addition (Figure 5C, green) leading us to conclude that the catalyst binding site is not near the Fd docking site on FNR.

To test whether the Co catalyst was binding at the NADP⁺ substrate binding site, NADP⁺ reduction assays were performed (Figure S7). Without bound catalyst, 230,000 TON h⁻¹ was observed while 180,000 TON h⁻¹ was observed with CoBF₂ catalyst bound. Since there is minimal difference in the NADP⁺ reduction rate upon catalyst binding, we conclude that the catalyst is not binding at the NADP⁺ binding site or blocking the entry of the substrate into the active site. In Figure 1C, His299, which does not block the NADP⁺ binding pocket and is located closest to the RuPS site on Fd (Cys 18) has been chosen as a representative binding site. Figure 6 shows the NADP⁺ bound structure of FNR (1GJR (Hermoso et al. 2002)). The positions of the histidines relative to the cofactor and substrate binding sites are highlighted.

We will use chemistry to refine the catalyst-protein binding. The beauty of this biohybrid system is that the molecular catalyst can be synthetically tuned. One target is cysteine modification with

thiol-reactive compounds. To this end, we investigated binding of a maleimide-functionalized cobaloxime to the engineered Cys residue (at position 402) of FNR. However, the preferential ligation of the available oxygen and nitrogen ligands to the axial Co ligation sites precluded covalent binding to the cysteine residue. Further synthetic development of catalysts that target cysteine residues is underway.

The current system provides an excellent platform for fine tuning and interrogating interprotein electron transfer reaction. Non-native cofactors can be incorporated into the binding pockets of the two protein system in order to alter the electron transfer pathway. The CoBF₂ catalyst binding site on FNR can be characterized by incorporating a cysteine-specific spin label (Poluektov et al. 2003) using the engineered Cys residue (at position 402) coupled with EPR spectroscopy for distance measurements. The distance between the RuPS and CoBF₂ catalyst is quite high (25.6 Å) in our model generated from the *Anabaena* crystal structure (Morales et al. 2000b). It is likely that the actual distance in the effective complex is much lower since the Fd:FNR encounter complex is already primed to undergo reorientation after initial binding. Site-directed mutagenesis can also be carried out on both protein partners to study the effects on electron transfer. Recently, site-directed mutagenesis on *Synechocystis* PCC 6803 Fd and FNR has been shown to affect electron transfer from reduced Fd to either FNR or hydrogenase (Wiegand et al. 2018).

Conclusions

This work provides an important example of incorporating synthetic molecules to creatively use and probe Nature's mechanisms. Here, we have developed a highly active two protein biohybrid system for photocatalytic H₂ production that uses interprotein electron transfer to achieve catalysis.

Ferredoxin (Fd) is used as a scaffold for binding of a ruthenium photosensitizer and attachment of cobaloxime molecules to FNR provides H₂ catalytic function. In this manner, we have reengineered the inherent interprotein electron transfer reaction in the photosynthetic pathway to make it photocatalytic for H₂ production. This work provides important insight into how to incorporate catalytic function into larger photosynthetic relays, such as thylakoid systems (Utschig et al. 2018). Likewise, interprotein schemes may provide a good strategy for accomplishing photocatalytic reduction of N₂ (Brown et al. 2016) and CO₂ (Miller et al. 2019; Woolerton et al. 2010), replacing light-sensitive nanoparticle materials. Continued work on photosynthetic-inspired biohybrids will provide an opportunity for breakthroughs in the resolution of fundamental mechanisms for coupling photons to proton-coupled electron transfer reactions, a necessary step forward in the development of optimized systems for capturing and converting the sun's energy into a storable fuel.

Acknowledgments

This work is supported by the U.S. Department of Energy Office of Science, Office of Basic Energy Sciences, Division of Chemical Sciences, Geosciences, and Biosciences, under Contract No. DE-AC02-06CH11357.

Conflict of Interest The authors declare that they have no conflict of interest.

References

Alstrum-Acevedo JH, Brennaman MK, Meyer TJ (2005) Chemical approaches to artificial photosynthesis. 2. *Inorg Chem* 44:6802-6827

Bakac A, Brynildson ME, Espenson JH (1986) Characterization of the structure, properties, and reactivity of a cobalt(II) macrocyclic complex. *Inorg Chem* 25:4108-4114

Bakac A, Espenson JH (1984) Unimolecular and bimolecular homolytic reactions of organochromium and organocobalt complexes. Kinetics and equilibria. *J Am Chem Soc* 106:5197-5202

Binda C, Coda A, Aliverti A, Zanetti G, Mattevi A (1998) Structure of the mutant E92K of [2Fe-2S] Ferredoxin I from *Spinacia oleracea* at 1.7 Å resolution. *Acta Crystallogr Sect D Biol Crystallogr* 54:1353-1358

Brown KA, Harris DF, Wilker MB, Rasmussen A, Khadka N, Hamby H, Keable S, Dukovic G, Peters JW, Seefeldt LC, King PW (2016) Light-driven dinitrogen reduction catalyzed by a CdS:nitrogenase MoFe protein biohybrid. *Science* 352:448-450

Cammack R, Rao KK, Barger CP, Hutson KG, Andrew PW, Rogers LJ (1977) Midpoint redox potentials of plant and algal ferredoxins. *Biochem J* 168:205

Corrado ME, Aliverti A, Zanetti G, Mayhew SG (1996) Analysis of the oxidation-reduction potentials of recombinant Ferredoxin-NADP⁺ reductase from spinach chloroplasts. *Eur J Biochem* 239:662-667

Diakonova A, Khrushchev S, Kovalenko I, Riznichenko GY, Rubin A (2016) Influence of pH and ionic strength on electrostatic properties of ferredoxin, FNR, and hydrogenase and the rate constants of their interaction. *Phys Biol* 13:056004

Faro M, Gómez-Moreno C, Stankovich M, Medina M (2002) Role of critical charged residues in reduction potential modulation of ferredoxin-NADP⁺ reductase. *Eur J Biochem* 269:2656-2661

Gould S, Strouse GF, Meyer TJ, Sullivan BP (1991) Formation of thin polymeric films by electropolymerization. Reduction of metal complexes containing bromomethyl-substituted derivatives of 2, 2'-bipyridine. *Inorg Chem* 30:2942-2949

Greenbaum E (1988) Interfacial photoreactions at the photosynthetic membrane interface: an upper limit for the number of platinum atoms required to form a hydrogen-evolving platinum metal catalyst. *J Phys Chem* 92:4571-4574

Grimme RA, Lubner CE, Bryant DA, Golbeck JH (2008) Photosystem I/molecular wire/metal nanoparticle bioconjugates for the photocatalytic production of H₂. *J Am Chem Soc* 130:6308-6309

Hermoso JA, Mayoral T, Faro M, Gómez-Moreno C, Sanz-Aparicio J, Medina M (2002) Mechanism of coenzyme recognition and binding revealed by crystal structure analysis of Ferredoxin–NADP⁺ reductase complexed with NADP⁺. *J Mol Biol* 319:1133-1142

Hurley JK, Morales R, Martínez-Júlvez M, Brodie TB, Medina M, Gómez-Moreno C, Tollin G (2002) Structure–function relationships in *Anabaena* ferredoxin/ferredoxin:NADP⁺ reductase electron transfer: insights from site-directed mutagenesis, transient absorption spectroscopy and X-ray crystallography. *Biochimica et Biophysica Acta (BBA) - Bioenergetics* 1554:5-21

Ihara M, Nishihara H, Yoon K-S, Lenz O, Friedrich B, Nakamoto H, Kojima K, Honma D, Kamachi T, Okura I (2006) Light-driven hydrogen production by a hybrid complex of a [NiFe]-Hydrogenase and the cyanobacterial Photosystem I. *Photochem Photobiol* 82:676-682

Iwuchukwu IJ, Vaughn M, Myers N, O'Neill H, Frymier P, Bruce BD (2010) Self-organized photosynthetic nanoparticle for cell-free hydrogen production. *Nat Nanotechnol* 5:73-79

Kohler L, Niklas J, Johnson RC, Zeller M, Poluektov OG, Mulfort KL (2019) Molecular Cobalt Catalysts for H₂ Generation with Redox Activity and Proton Relays in the Second Coordination Sphere. *Inorg Chem* 58:1697-1709

Kurusu G, Kusunoki M, Katoh E, Yamazaki T, Teshima K, Onda Y, Kimata-Arigo Y, Hase T (2001) Structure of the electron transfer complex between ferredoxin and ferredoxin-NADP⁺ reductase. *Nat Struct Biol* 8:117-121

Lewis NS (2007) Toward cost-effective solar energy use. *Science* 315:798-801

Lewis NS, Nocera DG (2006) Powering the planet: Chemical challenges in solar energy utilization. *Proc Natl Acad Sci USA* 103:15729

Lubner CE, Applegate AM, Knörzer P, Ganago A, Bryant DA, Happe T, Golbeck JH (2011) Solar hydrogen-producing bionanodevice outperforms natural photosynthesis. *Proc Natl Acad Sci USA* 108:20988

Lubner CE, Grimme R, Bryant DA, Golbeck JH (2010) Wiring Photosystem I for direct solar hydrogen production. *Biochemistry* 49:404-414

Martínez-Júlvez M, Hermoso J, Hurley JK, Mayoral T, Sanz-Aparicio J, Tollin G, Gómez-Moreno C, Medina M (1998) Role of Arg100 and Arg264 from *Anabaena* PCC 7119 Ferredoxin–NADP⁺ reductase for optimal NADP⁺ binding and electron transfer. *Biochemistry* 37:17680-17691

Medina M (2009) Structural and mechanistic aspects of flavoproteins: photosynthetic electron transfer from Photosystem I to NADP⁺. *FEBS J* 276:3942-3958

Miller M, Robinson WE, Oliveira AR, Heidary N, Kornienko N, Warnan J, Pereira IAC, Reisner E (2019) Interfacing formate dehydrogenase with metal oxides for the reversible electrocatalysis and solar-driven reduction of carbon dioxide. *Angew Chem Int Ed* 131:4649-4653

Morales R, Charon M-H, Kachalova G, Serre L, Medina M, Gómez-Moreno C, Frey M (2000a) A redox-dependent interaction between two electron-transfer partners involved in photosynthesis. *Photosynth Res* 66:271-276

Morales R, Kachalova G, Vellieux F, Charon M-H, Frey M (2000b) Crystallographic studies of the interaction between the ferredoxin-NADP⁺ reductase and ferredoxin from the cyanobacterium *Anabaena*: looking for the elusive ferredoxin molecule. *Acta Crystallogr Sect D Biol Crystallogr* 56:1408-1412

Mosebach L, Heilmann C, Mutoh R, Gäbelein P, Steinbeck J, Happe T, Ikegami T, Hanke G, Kurisu G, Hippler M (2017) Association of Ferredoxin:NADP⁺ oxidoreductase with the photosynthetic apparatus modulates electron transfer in *Chlamydomonas reinhardtii*. *Photosynth Res* 134:291-306

Mulfort KL, Utschig LM (2016) Modular Homogeneous Chromophore–Catalyst Assemblies. *Acc Chem Res* 49:835-843

Mulo P, Medina M (2017) Interaction and electron transfer between ferredoxin–NADP⁺ oxidoreductase and its partners: structural, functional, and physiological implications. *Photosynth Res* 134:265-280

Niklas J, Mardis KL, Rakhimov RR, Mulfort KL, Tiede DM, Poluektov OG (2012) The hydrogen catalyst cobaloxime: A multifrequency EPR and DFT study of cobaloxime's electronic structure. *J Phys Chem B* 116:2943-2957

Palma PN, Lagoutte B, Krippahl L, Moura JJG, Guerlesquin F (2005) *Synechocystis* ferredoxin/ferredoxin-NADP⁺-reductase/NADP⁺ complex: Structural model obtained by NMR-restrained docking. FEBS Lett 579:4585-4590

Poluektov OG, Utschig LM, Dalosto S, Thurnauer MC (2003) Probing local dynamics of the photosynthetic bacterial reaction center with a cysteine specific spin label. J Phys Chem B 107:6239-6244

Quaranta A, Lagoutte B, Frey J, Sétif P (2016) Photoreduction of the ferredoxin/ferredoxin-NADP⁺-reductase complex by a linked ruthenium polypyridyl chromophore. Photosynth Res 160:347-354

Silver SC, Niklas J, Du P, Poluektov OG, Tiede DM, Utschig L (2013) Protein delivery of a Ni catalyst to Photosystem I for light-driven hydrogen production. J Am Chem Soc 135:13246-13249

Soltau SR, Dahlberg PD, Niklas J, Poluektov OG, Mulfort KL, Utschig LM (2016) Ru-protein-Co biohybrids designed for solar hydrogen production: understanding electron transfer pathways related to photocatalytic function. Chem Sci 7:7068-7078

Soltau SR, Niklas J, Dahlberg PD, Mulfort KL, Poluektov OG, Utschig LM (2017) Charge separation related to photocatalytic H₂ production from a Ru-Apoflavodoxin-Ni biohybrid. ACS Energy Lett 2:230-237

Soltau SR, Niklas J, Dahlberg PD, Poluektov OG, Tiede DM, Mulfort KL, Utschig L (2015) Aqueous light driven hydrogen production by a Ru–ferredoxin–Co biohybrid. *Chem Commun* 51:10628-10631

Stoll S, Schweiger A (2006) EasySpin, a comprehensive software package for spectral simulation and analysis in EPR. *J Magn Reson* 178:42-55

Sun L, Berglund H, Davydov R, Norrby T, Hammarström L, Korall P, Börje A, Philouze C, Berg K, Tran A (1997) Binuclear ruthenium– manganese complexes as simple artificial models for Photosystem II in green plants. *J Am Chem Soc* 119:6996-7004

Utschig L, Soltau SR, Tiede DM (2015) Light-driven hydrogen production from Photosystem I-catalyst hybrids. *Curr Opin Chem Biol* 25:1-8

Utschig LM, Dimitrijevic NM, Poluektov OG, Chemerisov SD, Mulfort KL, Tiede DM (2011a) Photocatalytic hydrogen production from noncovalent biohybrid Photosystem I/Pt nanoparticle complexes. *J Phys Chem Lett* 2:236-241

Utschig LM, Silver SC, Mulfort KL, Tiede DM (2011b) Nature-driven photochemistry for catalytic solar hydrogen production: A Photosystem I–transition metal catalyst hybrid. *J Am Chem Soc* 133:16334-16337

Utschig LM, Soltau SR, Mulfort KL, Niklas J, Poluektov OG (2018) Z-scheme solar water splitting via self-assembly of Photosystem I-catalyst hybrids in thylakoid membranes. *Chem Sci* 9:8504-8512

Wiegand K, Winkler M, Rumpel S, Kannchen D, Rexroth S, Hase T, Farès C, Happe T, Lubitz W, Rögner M (2018) Rational redesign of the ferredoxin-NADP⁺-oxido-reductase/ferredoxin-interaction for photosynthesis-dependent H₂-production. *Biochimica et Biophysica Acta, Bioenergetics* 1859:253-262

Woolerton TW, Sheard S, Reisner E, Pierce E, Ragsdale SW, Armstrong FA (2010) Efficient and clean photoreduction of CO₂ to CO by enzyme-modified TiO₂ nanoparticles using visible light. *J Am Chem Soc* 132:2132-2133

Table 1: Photocatalytic turnover data for Fd-RuPS and FNR-CoBF₂ hybrid mixtures under different conditions

FNR-Co hybrid	Photosensitizer	[NaCl]	TOF (mol H₂ (mol FNR)⁻¹ h⁻¹)	TON (mol H₂ (mol FNR)⁻¹)
FNR-CoBF ₂ (1.9 μM)	Fd-RuPS (4 equiv.)	0.2 M	110	490
FNR-CoBF ₂ (0.4 μM)	Fd-RuPS (21 equiv.)	0.2 M	330	1640
FNR-CoBF ₂ (0.1 μM)	Fd-RuPS (72 equiv.)	0.2 M	550	2780
ApoFNR-CoBF ₂	Fd-RuPS (4 equiv.)	0.2 M	110	510
FNR-CoBF ₂	ApoFd-RuPS (4 equiv.)	0.2 M	130	490
ApoFNR-CoBF ₂	ApoFd-RuPS (4 equiv.)	0.2 M	160	740
FNR-CoBF ₂	Fd-RuPS (4 equiv.)	None	50	220
FNR-CoBF ₂	Fd-RuPS (4 equiv.)	1.0 M	30	140

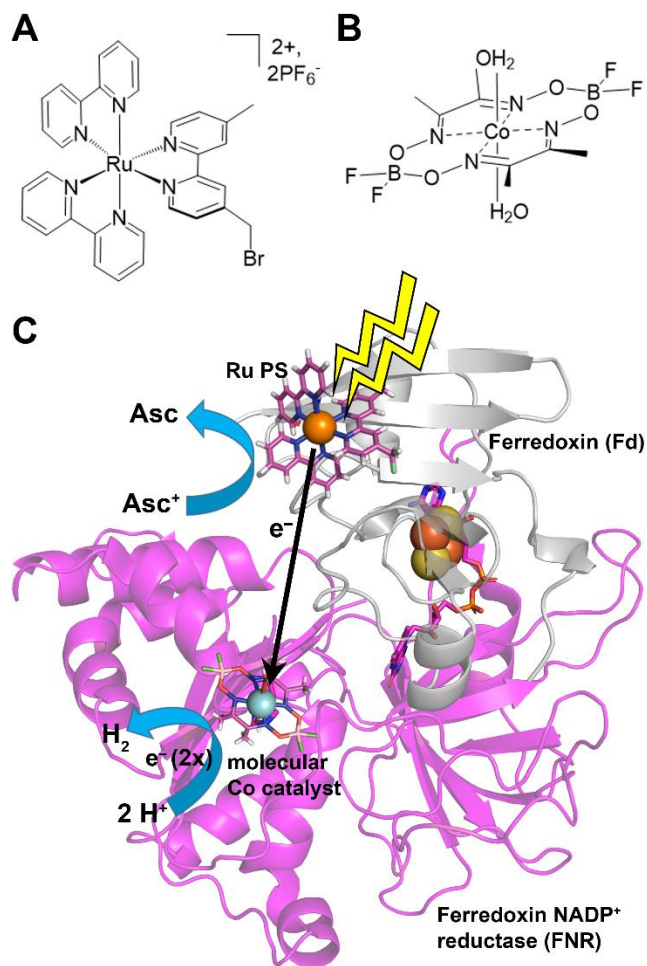


Figure 1: Light driven H_2 production via intermolecular electron transfer. Chemical structures of (A) ruthenium photosensitizer (RuPS), $[Ru(4-CH_2Br-4'-CH_3-2,2'-bpy)(bpy)_2] \cdot 2PF_6$; and (B) cobaloxime catalyst ($CoBF_2$), $Co(dmgbf_2)_2 \cdot 2H_2O$ used in the study. (C) Proposed photocatalytic H_2 generation scheme by direct intermolecular electron transfer from the PS on the Fd-RuPS hybrid to the $CoBF_2$ catalyst on the FNR- $CoBF_2$ hybrid. Spinach Ferredoxin structure (1A70) has been aligned with the *Anabaena* FNR:Ferredoxin complex structure (1EWY) to generate the docked structure.

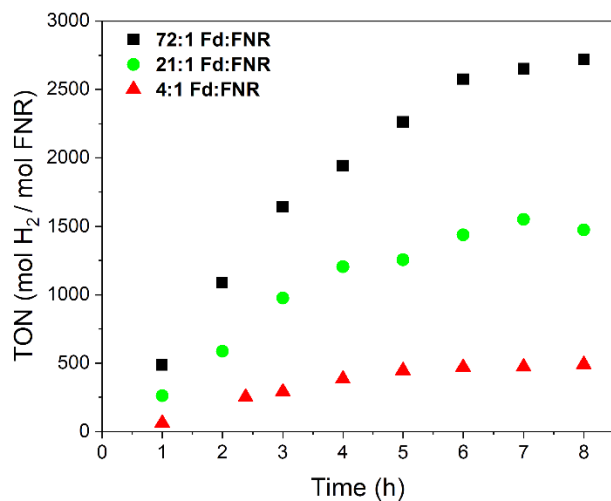


Figure 2: Time course profile of H₂ production from different mixtures of Fd-RuPS and FNR-CoBF₂ hybrids under blue LED illumination. The concentration of Fd-RuPS hybrid was maintained at 8 μM while the concentration of the FNR-CoBF₂ hybrid was (black squares) 0.1 μM; (green circles) 0.4 μM; and (red triangles) 1.9 μM. The reaction was performed in 10 mM MES, pH 6.1 with 200 mM NaCl and 100 mM sodium ascorbate.

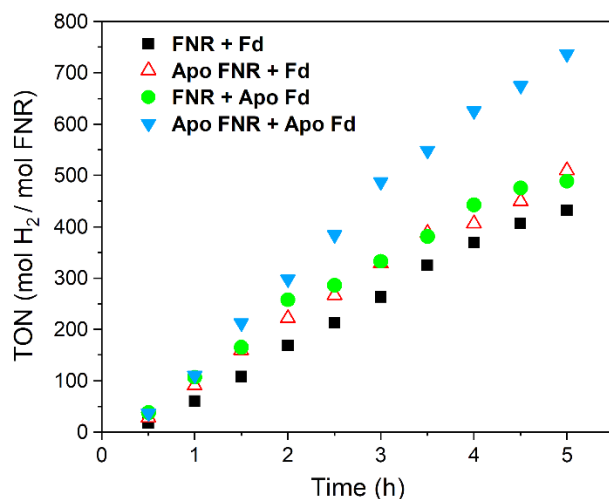


Figure 3: Time course profiles of photocatalytic H₂ production with different cofactor content of the Fd-RuPS and FNR-CoBF₂ hybrids. The [2Fe-2S] cluster of Fd and FAD cofactor of FNR were each removed, and different combinations of the resultant hybrids were investigated to determine the cofactor involvement in photocatalysis. The PS:catalyst ratio was maintained at 4:1 for all the experiments. The conditions tested were (black, squares) Fd-RuPS (with [2Fe-2S] cluster) and FNR-CoBF₂ (with FAD) hybrids; (empty red triangles) Fd-RuPS (with [2Fe-2S] cluster) and ApoFNR-CoBF₂ (no FAD) hybrids; (green circles) ApoFd-RuPS (no [2Fe-2S] cluster) and FNR-CoBF₂ (with FAD) hybrids; and (blue inverted triangles) ApoFd-RuPS (no [2Fe-2S] cluster) and ApoFNR-CoBF₂ (no FAD) hybrids. Data shown in (black, squares) reproduced from Figure 2 (red triangles). The assay conditions were the same as that for the experiments in Figure 2.

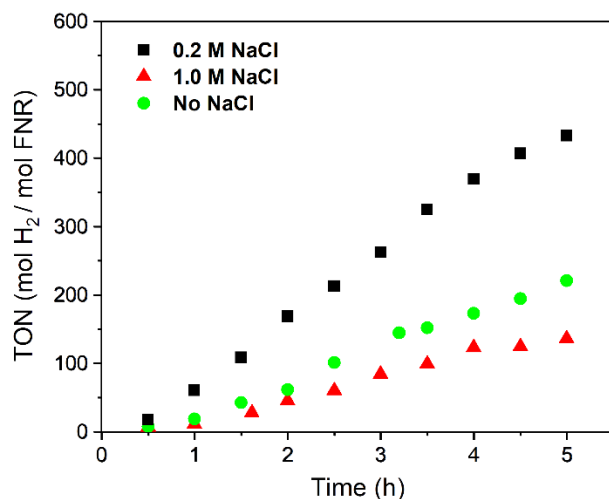


Figure 4: Effect of ionic strength on photocatalytic H₂ production with 4:1 Fd-RuPS:FNR-CoBF₂ hybrid mixtures under blue LED illumination. The Fd-RuPS concentration was 8 μM and FNR-COBF₂ was 2 μM. Assay conditions were 10 mM MES, pH 6.1 with 100 mM sodium ascorbate and (black squares) 200 mM NaCl; (green circles) no NaCl; and (red triangles) 1 M NaCl. Data shown in (black squares) reproduced from Figure 2 (red triangles) and Figure 3 (black squares). Besides the variation in salt concentration, all other assay conditions were the same as that for Figure 2.

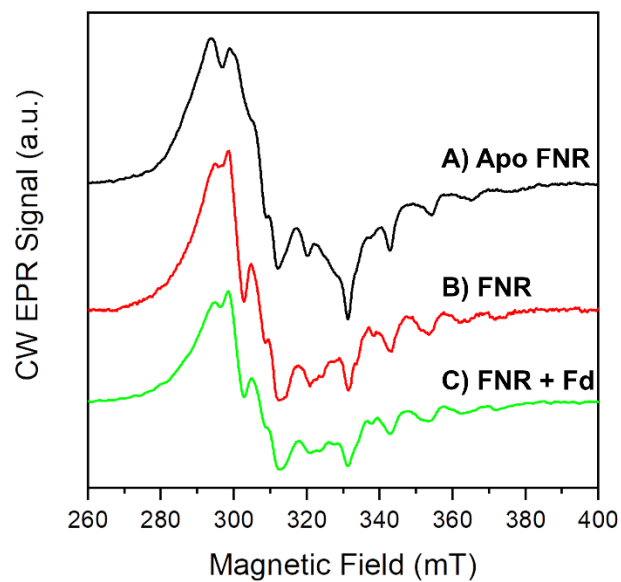


Figure 5: CW X-band EPR spectra of (A) ApoFNR-CoBF₂ hybrid; (B) FNR-CoBF₂ hybrid; and (C) 1:1 mixture of FNR-CoBF₂ hybrid and spinach Ferredoxin. Assay buffer contained 20 mM HEPES, pH 7.9 and 100 mM sodium ascorbate. All EPR spectra were obtained at 20 K.

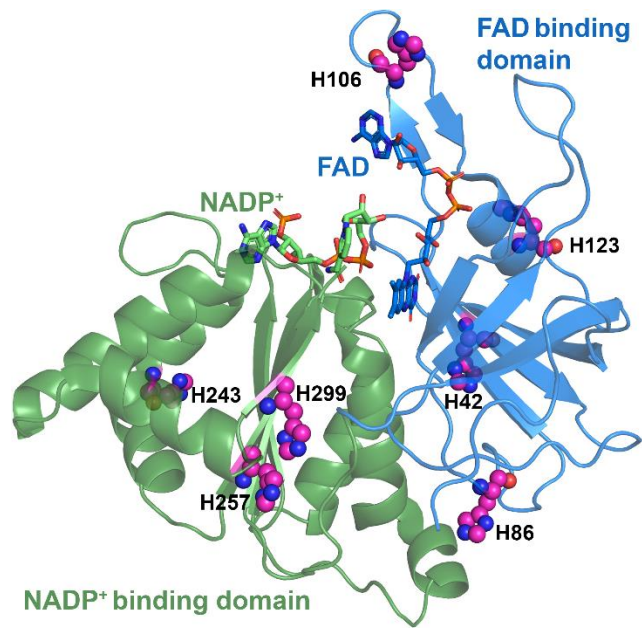


Figure 6: Structure of *Anabaena* FNR with NADP⁺ bound at the active site (1GJR). The FAD (blue sticks) and NADP⁺ (green sticks) binding domains are shown in blue and green, respectively. The 7 His found in the structure are shown as magenta spheres (His7 is missing in the crystal structure).